International Journal of Applied Earth Observation and Geoinformation 118 (2023) 103239

Contents lists available at ScienceDirect

International Journal of Applied Earth Observation and Geoinformation

journal homepage: www.elsevier.com/locate/jag

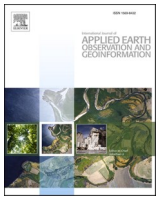

Exploring the largest known Bronze Age earthworks in Europe through medium resolution multispectral satellite images

Athos Agapiou [a,*], Alexandru Hegyi [b,c], Florin Gogâltan [d], Andrei Stavilă [e], Victor Sava [f], Apostolos Sarris [g], Cristian Floca [h], Leonard Dorogostaisky [i]

[a] Earth Observation Cultural Heritage Research Lab, Department of Civil Engineering and Geomatics, Faculty of Engineering and Technology, Cyprus University of Technology, Limassol 3036, Cyprus
[b] Centre for Southeast Asian Studies, Kyoto University, 46 Shimo-Adachi, Yoshida, Sakyo-ku, 606-8501 Kyoto, Japan
[c] Applied Geomorphology and Interdisciplinary Research Centre (CGACI), Department of Geography, West University of Timişoara, 300223 Timişoara, Timis, Romania
[d] Institute of Archaeology and History of Art of Cluj-Napoca, Romania
[e] Faculty of Letters, History and Theology, West University of Timişoara, Vasile Pârvan Blvd. no.4, Timişoara 300223, Romania
[f] Arad Museum Complex, George Enescu, 1, 3010131 Arad, Romania
[g] Digital Humanities GeoInformatics Lab., Archaeological Research Unit (ARU), Department of History and Archaeology, University of Cyprus, Nicosia 1678, Cyprus
[h] Institute of Banat Studies "Titu Maiorescu", Romanian Academy-Timişoara Branch, Mihai Viteazu Blvd, no. 24, Timişoara 300223, Romania
[i] "ArheoVest" Association, Leonard Nicolae Street, no. 2, ap. 2, Timişoara 300454, Romania

ARTICLE INFO

Keywords:
Remote sensing archaeology
Crop mark
Archaeological prospection
Vegetation
Indices
Fortifications
Romania

ABSTRACT

This study aims to provide new insights into Europe's largest known Bronze Age earthworks using open-access and freely distributed medium resolution satellite images. The most extensive Bronze Age fortifications in Europe, namely, the Cornești-Iarcuri and Sântana – Cetatea Veche sites, were investigated through the Sentinel 2 and the newly launched Landsat 9 optical sensors. Image processing techniques were applied to both datasets, including vegetation indices, orthogonal spectral transformations, and pan-sharpening techniques. The final results revealed several known and unknown archaeological proxies by enhancing a number of linear and curved crop marks in the vicinity of the archaeological sites. Indeed, while previously implemented geophysical results confirmed some of these archaeological proxies, new findings (crop marks) were also revealed, representing archaeological structures that were unknown until now. The study's overall findings indicate that medium resolution satellite images can be used in appropriate areas with archaeological interest as a first step toward better understanding the broader context of an area. The findings addressed in this study have a direct impact on the non-invasive aspect of archaeology, as the methodology employed in this paper may be applied to various types of sites in southwestern Romania and beyond and might serve as a solid starting point for any archaeological project. Finally, this is the first elaboration of Landsat 9 intended for archaeological research and our study proves that its utility for archaeological and heritage purposes.

1. Introduction

Satellite observations can support archaeological research, allowing many previously unknown sites to be discovered (Luo et al., 2019). At the beginning of the 21st century, once satellite and high-resolution images became widely available, archaeologists and archaeology enthusiasts began searching for ground anomalies, some of which have been identified as archaeological sites and others which have remained a topic of contention. However, satellite remote sensing can provide more than visual recognition of archaeological remains (Parcak, 2009). Spaceborne imagery may aid in comprehending a larger context or even prior human actions. For example, researchers deduced from a series of satellite images what paths humans had used to move the megaliths of Easter Island (Lipo and Hunt, 2005) and used satellite imagery to better understand the impressive Nazca geoglyphs (Masini and Lasaponara, 2020).

* Corresponding author.
E-mail addresses: athos.agapiou@cut.ac.cy (A. Agapiou), alexandru.hegyi@e-uvt.ro, hegyi@cseas.kyoto-u.ac.jp (A. Hegyi), floringogaltan@gmail.com (F. Gogâltan), andrei.stavila@e-uvt.ro (A. Stavilă), sava_vic@yahoo.com (V. Sava), asarri01@ucy.ac.cy (A. Sarris), cfloca87@gmail.com (C. Floca), ldoro1959@gmail.com (L. Dorogostaisky).

https://doi.org/10.1016/j.jag.2023.103239
Received 20 May 2022; Received in revised form 17 February 2023; Accepted 18 February 2023
Available online 24 February 2023

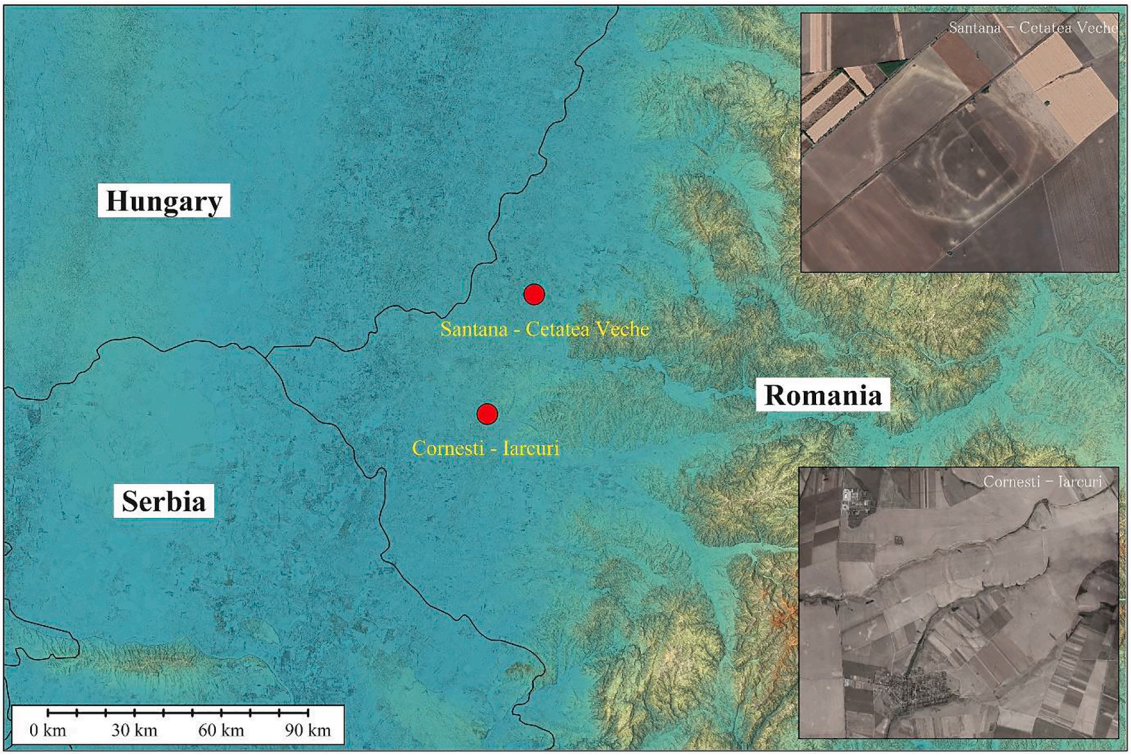

Fig. 1. The Bronze Age fortifications discussed in this paper (Background: ASTER GDEM v3 Worldwide Elevation Data 1 arc-second resolution; satellite image screenshots for both of the sites: Google Earth captures).

Fig. 2. Cornești-Iarcuri: a. Phase B of the first rampart construction (after Szentmiklosi et al. 2011, Fig. 7); b. The profile of the defence ditch of the fourth enclosure (after Szentmiklosi et al. 2016, Fig. 4.1); c. The plan of the internal structure of the first rampart illustrates the two phases of construction (after Szentmiklosi et al. 2011, Fig. 5); d. Aerial photography of the Cornești-Iarcuri fortification (after Szentmiklosi et al., 2011, Fig. 2).

Recent studies, indicate a continuous growth of remote sensing in archaeological research. For instance, the integration of artificial intelligence algorithms and big remote sensing data is considered a very promising topic for the next century (Luo et al., 2022; Argyrou and Agapiou 2022). Studies in the last years argue that the employment of multi-platform remote sensing sensors can provide significant improvement in the efficiency and accuracy for the detection of archaeological sites (Luo et al., 2023; Opitz and Herrmann 2018).

There are various potential applications of remote sensing technologies, and archaeology has benefited from its more complex applications, resulting in the rapid, substantial growth of novel approaches, primarily in landscape archaeology (Hritz, 2014; Yang et al., 2022). Regardless if the sensor is passive or active or produces panchromatic or multispectral datasets, in the last decades, remote sensing in archaeology has become more analytical, opening the way to what is now known in the scientific literature as space or satellite-based archaeology (Luo et al., 2019; Agapiou and Lysandrou, 2015). The free and almost near real-time availability of optical and radar satellite imagery (i.e., Earth Explorer, Sentinel Hub) has increased the number of its applications in archaeology and cultural heritage (see examples in Chen et al., 2015; Tapete and Cigna, 2018; Zanni and de Rosa, 2019; Abate and Lasaponara, 2019; Fanti et al., 2013).

Vegetation and soil anomalies – as a result of buried archaeological remains – can be detected through the processing of multispectral images. The so-called "crop mark" – a phenomenon of stressed vegetation that overlays shallow buried archaeological features – has been extensively explored through satellite and aerial sensors (Reid, 2016; Agapiou et al., 2012; Calleja et al., 2018; Kirk et al., 2016; Holliday and Gartner, 2007). Buried archaeological remains may cause a long-term chemical change in the soil, affecting plant growth in those locations (Holliday and Gartner, 2007; Malhotra et al., 2018), so crop mark anomalies can be detected. In most cases, the spectral difference between healthy vegetation and crop marks needs to be enhanced using a different spectrum beyond the visible one (i.e., the NIR part of the spectrum).

This image-based detection is usually applied through commercial high- or very high-resolution imageries (Agapiou, 2017a) rather than medium -and often freely distributed- images. As Abate et al. (2020) argue, except for a few examples, the spatial resolution of medium resolution sensors that provide freely distributed datasets is still challenging for archaeological purposes. Indeed, despite the open access policy, the Sentinel and Landsat series were limitedly applied in the past for detecting archaeological proxies (but see Tapete and Cigna, 2018; Agapiou et al., 2014). This is also indicated in the literature as most

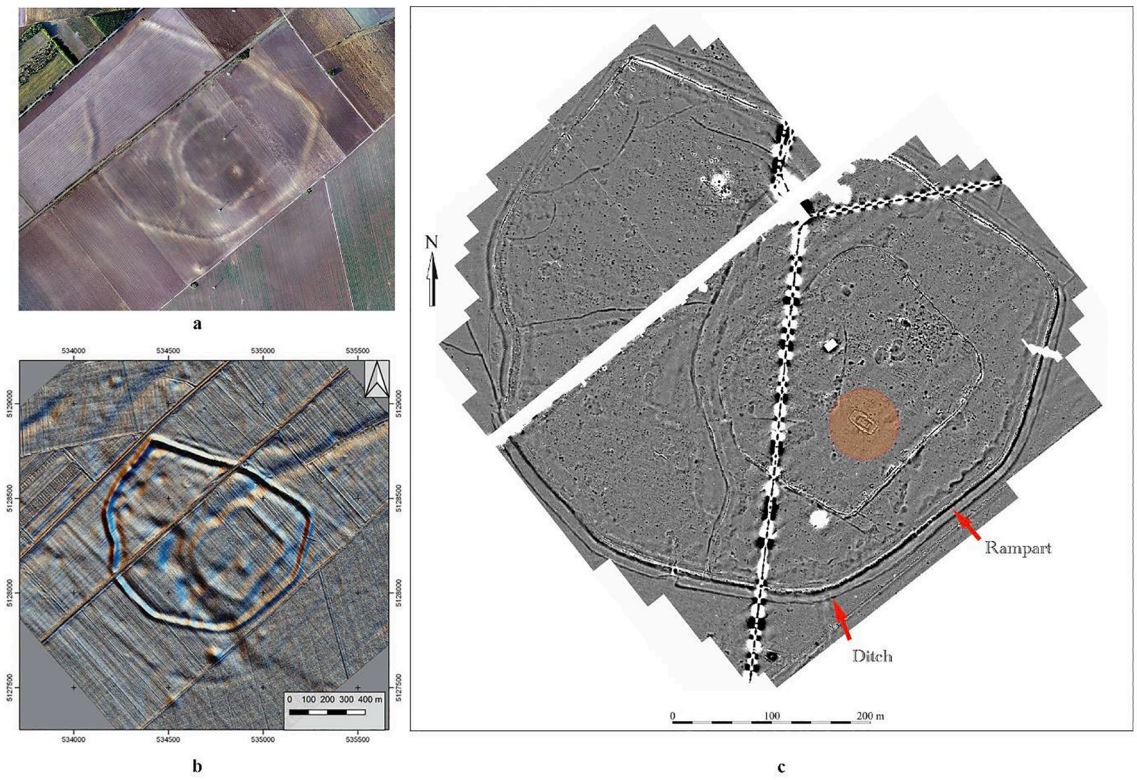

Fig. 3. Sântana – Cetatea Veche: a. Orthophoto map; b. LiDAR Digital Elevation Model (after Gogâltan et al., 2019, Fig. 11); c. Magnetic survey results (after Gogâltan et al., 2019, Fig. 5).

Table 1
Images used in this study.

No.	Satellite	Product Name	Acq. date	Res. (m)
1.	Landsat 9	LC09_L2SP_186028_20220319_20220323_02_T1	2022–03-19	30
2.	Landsat 9	LC09_L1TP_186028_20220319_20220322_02_T1	2022–03-19	15
3.	Sentinel 2B	S2B_MSIL2A_20220322T093029_N0400_R136_T34TES_20220322T123322	2022–03-22	10
4.	Sentinel 2B	S2B_MSIL2A_20220325T094029_N0400_R036_T34TDR_20220325T132010	2022–03-25	10
5.	Sentinel 2B	S2B_MSIL2A_20220325T094029_N0400_R036_T34TDS_20220325T132010	2022–03-25	10
6.	Sentinel 2A	S2A_MSIL2A_20181014T093031_N0209_R136_T34TES_20181014T111722	2018–10-14	10
7.	Sentinel 2B	S2B_MSIL2A_20220210T093029_N0400_R136_T34TER_20220210T113151	2020–02-10	10
8.	Sentinel 2B	S2B_MSIL2A_20220312T093029_N0400_R136_T34TES_20220312T122913	2022–03-12	10

research activities are usually supported by higher resolution and, more often, commercial satellite sensors such as those provided by the WorldView, IKONOS, and Planet Dove constellations (Masini and Lasaponara, 2020; Chen et al., 2015).

The aim of this study is therefore two-fold: on the one hand to contribute to this open discussion regarding the potentials and limitations of medium resolution sensors like those of the Sentinel 2 and the newly launched Landsat 9 for archaeological research and, on the other hand, to explore their potentials through a series of image processing techniques for the detection of archaeological proxies.

2. Case study area

The study is focused on sites that have been thoroughly investigated in the past using non-invasive methods and archaeological excavations. These sites are part of long-term systematic archaeological investigations of the authors of this study, hence providing a unique prospect to directly link the results of image analysis and archaeological investigations. The largest fortifications of the European Bronze Age were built after 1500 BCE in a small region of about 12,000 km^2 between the confluence of the Tisza and Mureș rivers (southeast of the Pannonian Plain). Located in a low plain area (Fig. 1), they covered areas ranging from fifteen to over 1700 ha (Gogâltan and Sava, 2010). A habitat-friendly environment, where multi-layered settlements (tells) of the Middle Bronze Age (ca. 2000/1900–1600/1500 BCE) had also thrived 50–100 years before, was thus exploited. The tells were much smaller (about 1 ha) and rarely reached up to 8 ha with the so-called satellite settlement (Sava and Gogâltan, 2022). Impressive ditches also surrounded the tells.

The Bronze Age fortifications of this region can be labelled as mega-forts, a term coined by Harding (2017) and which have only been investigated in the last ten to fifteen years. Archaeological excavations of mega-forts have been carried out in Cornești (Szentmiklosi et al., 2011) (Fig. 2), Sântana (Gogâltan et al., 2019) (Fig. 3), and Munar (Sava and Gogâltan, 2017) in Romania, Csanádpalota (Szeverényi et al., 2017) and Makó – Rákos-Császár (Szeverényi et al., 2017) in Hungary, and Gradište Idjoš in Serbia (Molloy et al., 2020).

3. Data and methodology

3.1. Data

For the purposes of the study, medium resolution multispectral images were used with a spatial resolution ranging between 10 and 30 m.

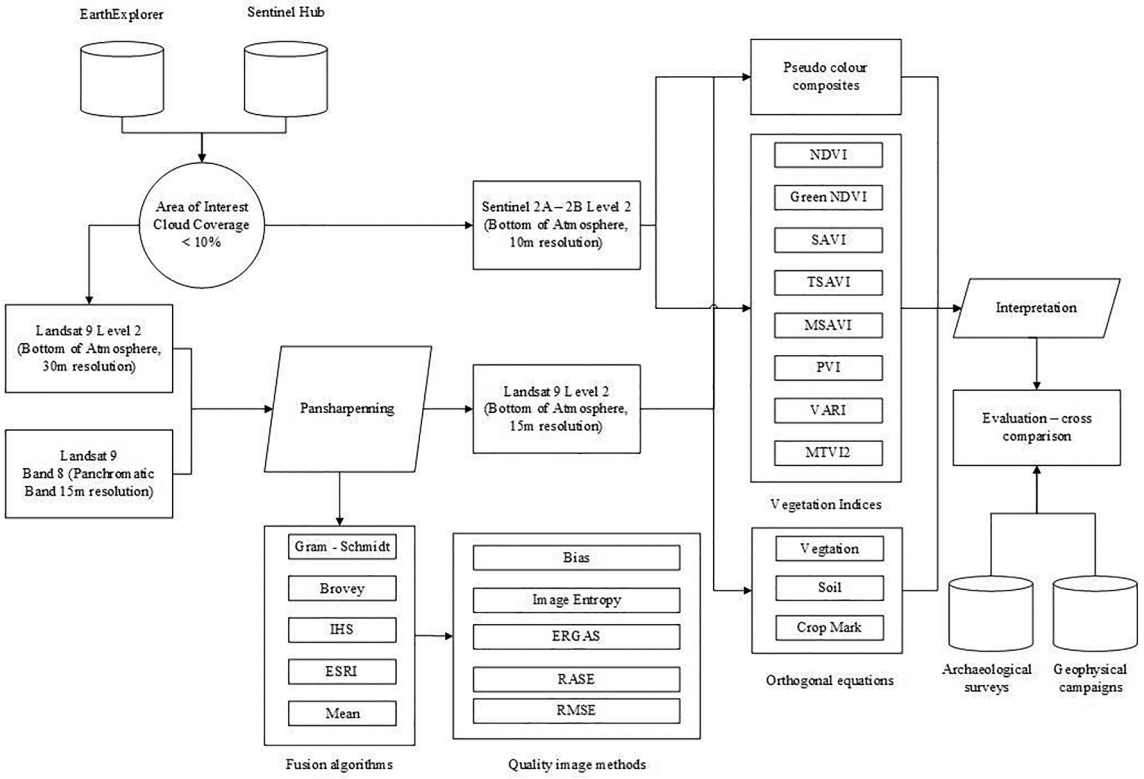

Fig. 4. The overall methodology of the current study.

Table 2
Vegetation indices used in this study.

Vegetation Index Name	Veg. Index	Equation	Reference	equation
Normalized Difference Vegetation Index	NDVI	$(p_{NIR} - p_{red})/(p_{NIR} + p_{red})$	Rouse et al. (1974)	[eq. 2]
Green Normalized Difference Vegetation Index	Green NDVI	$(p_{NIR} - p_{green})/(p_{NIR} + p_{green})$	Gitelson et al. (1996)	[eq. 3]
Soil Adjusted Vegetation Index	SAVI	$(1 + L)*(p_{NIR} - p_{red})/(p_{NIR} + p_{red} + L)$	Huete (1988)	[eq. 4]
Transformed Soil Adjusted Vegetation Index	TSAVI	$[\alpha(p_{NIR}-\alpha\, p_{NIR} - b)]/[(p_{red} + \alpha\, p_{NIR} - \alpha b + 0.08\,(1 + \alpha^2))]$ $p_{NIR,soil} = \alpha\, p_{red,soil} + b$	Baret and Guyot (1991)	[eq. 5]
Modified Soil Adjusted Vegetation Index	MSAVI	$[2\, p_{NIR} + 1-[(2\, p_{NIR} + 1)^2-8(p_{NIR} - p_{red})]^{1/2}]/2$	Qi et al. (1994)	[eq. 6]
Perpendicular Vegetation Index	PVI	$(p_{NIR} - \alpha\, p_{red} - b)/(1 + \alpha^2)$ $p_{NIR,soil} = \alpha\, p_{red,soil} + b$	Richardson and Wiegand (1977)	[eq. 7]
Visible Atmospherically Resistant Index	VARI	$(p_{Green} - p_{red})/(p_{Green} + p_{red} - p_{Blue})$	Gitelson et al. (2002)	[eq. 8]
Modified Triangular Vegetation Index	MTVI2	$[1.5(1.2*(p_{NIR} - p_{green}) - 2.5(p_{Red} - p_{green})]/[(2\, p_{NIR} + 1)^2 - (6\, p_{NIR} - 5\, p_{Red}^{0.5}) - 0.5]^{0.5}$	Haboudane et al. (2004)	[eq. 9]
Simple Ratio	SR	p_{NIR}/p_{red}	Jordan (1969)	[eq. 10]

We explored optical images from the Copernicus Sentinel-2 sensors (2A and 2B) and images from the newly launched sensor from NASA and the USGS, namely, the Landsat 9 sensor. As mentioned earlier, this is the first time that this specific sensor (Landsat 9) has been analysed for archaeological prospection purposes. The following images were used in this study, as shown in Table 1.

Landsat 9 and Sentinel 2 images were obtained from the Earth-Explorer and Sentinel Hub cloud platforms, respectively. The area of interest was defined, while limits to cloud coverage (<10%) were applied. The 30-m spatial resolution Landsat image was downloaded at Level 2 (surface reflectance), minimising errors due to radiometric and atmospheric conditions. For the same product, the panchromatic band of the Landsat (band 8, 15-m resolution) was also acquired. Sentinel 2 images were acquired (Bottom-Of-Atmosphere products) with a spatial resolution of 10 m (for the visible and NIR bands).

3.2. Methodology

The overall methodology of the study is presented in Fig. 4. Once the images were downloaded, they were imported into the ArcGIS Pro environment for further processing. Then, various pan-sharpening methods were applied to the Landsat 9 multispectral bands in order to be downscaled to 15-m resolution. This step included four different pan-sharpening methods as follows: (a) the Gram–Schmidt method; (b) the Brovey transformation; (c) the principal component analysis, in short PCA, and (d) the hue-saturation-value (HSV) transformation.

The Gram-Schmidt algorithm is an image processing technique that improves the spatial resolution of the multispectral bands using a higher spatial resolution image (panchromatic). The Gram-Schmidt algorithm is applied on the high-resolution band and multispectral spectral bands (Laben and Brower, 2000). The Brovey transformation is a widely used fusion technique proposed by Zhang (2004), which is a low-computational process and easy to implement (Johnson et al., 2014). The new pan-sharpened image combines only three spectral bands from the input scene at a time. The Brovey transformation is given below in

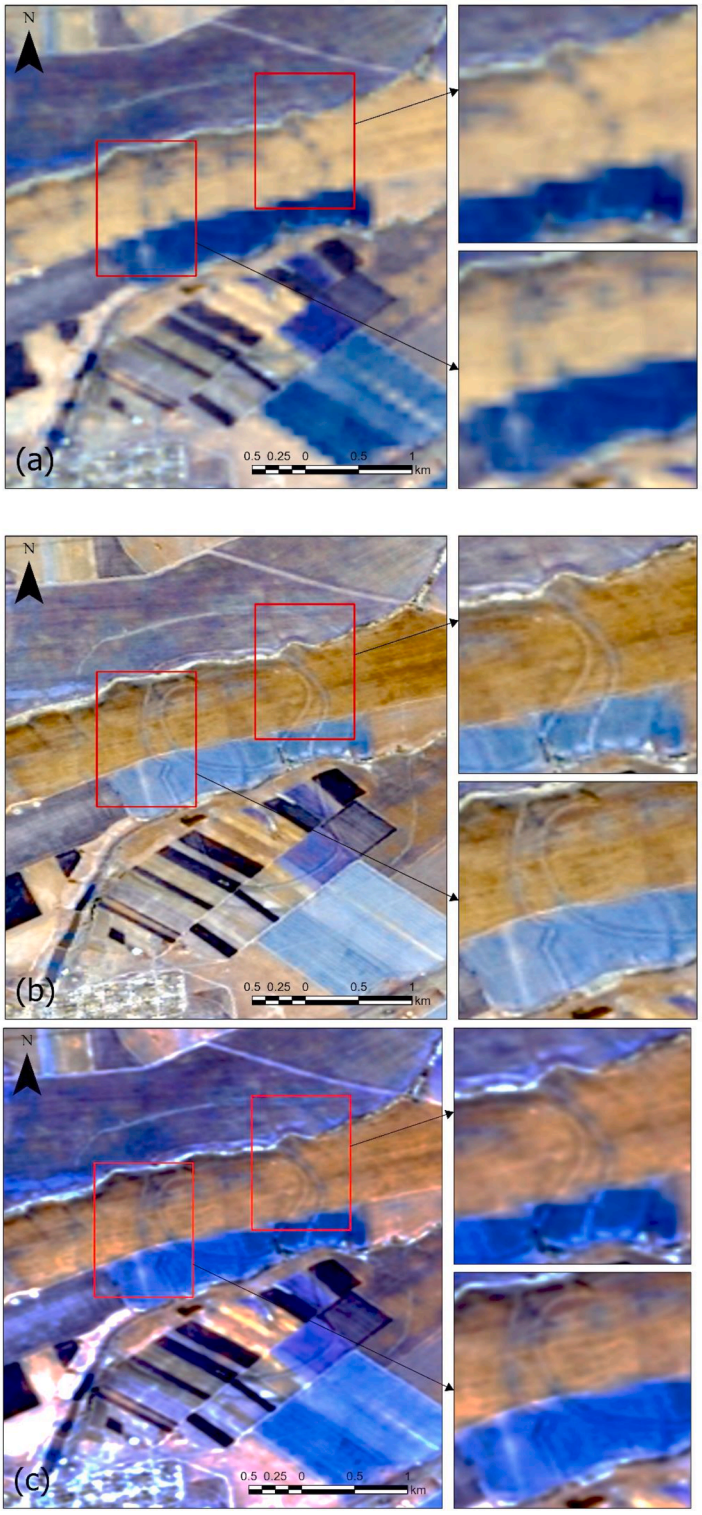

Fig. 5. (a) Landsat 9 30-m resolution over the archaeological site of Cornești-Iarcuri. (b) Pan-sharpened Landsat image at 15-m resolution using the Brovey transformation and (c) the Gramm-Schmidt transformation. Curved features (crop marks) are evident in both pan-sharpening techniques.

equation 1:

$$\text{Red} = \text{High Resolution}_{\text{Pan}} * \text{Low}_{\text{Red Band}} / (\text{Low}_{\text{Red Band}} + \text{Low}_{\text{Green Band}} + \text{Low}_{\text{Blue Band}}).$$

$$\text{Green} = \text{High Resolution}_{\text{Pan}} * \text{Low}_{\text{Green Band}} / (\text{Low}_{\text{Red Band}} + \text{Low}_{\text{Green Band}} + \text{Low}_{\text{Blue Band}}).$$

$$\text{Blue} = \text{High Resolution}_{\text{Pan}} * \text{Low}_{\text{Blue Band}} / (\text{Low}_{\text{Red Band}} + \text{Low}_{\text{Green Band}} + \text{Low}_{\text{Blue Band}}) \text{ [eq. 1].}$$

Regarding the hue-saturation-value (HSV) fusion model, the first component denotes the pure colour, while the second component denotes the level of saturation at a constant lightness. The last component refers to its brightness. The RGB image is converted to HSV colour space using the HSV method. At the same time, the value band is replaced with a high-resolution image (Nikolakopoulos, 2008; Ehlers et al., 2010).

Finally, the so-called ESRI pan-sharpening method was applied. This

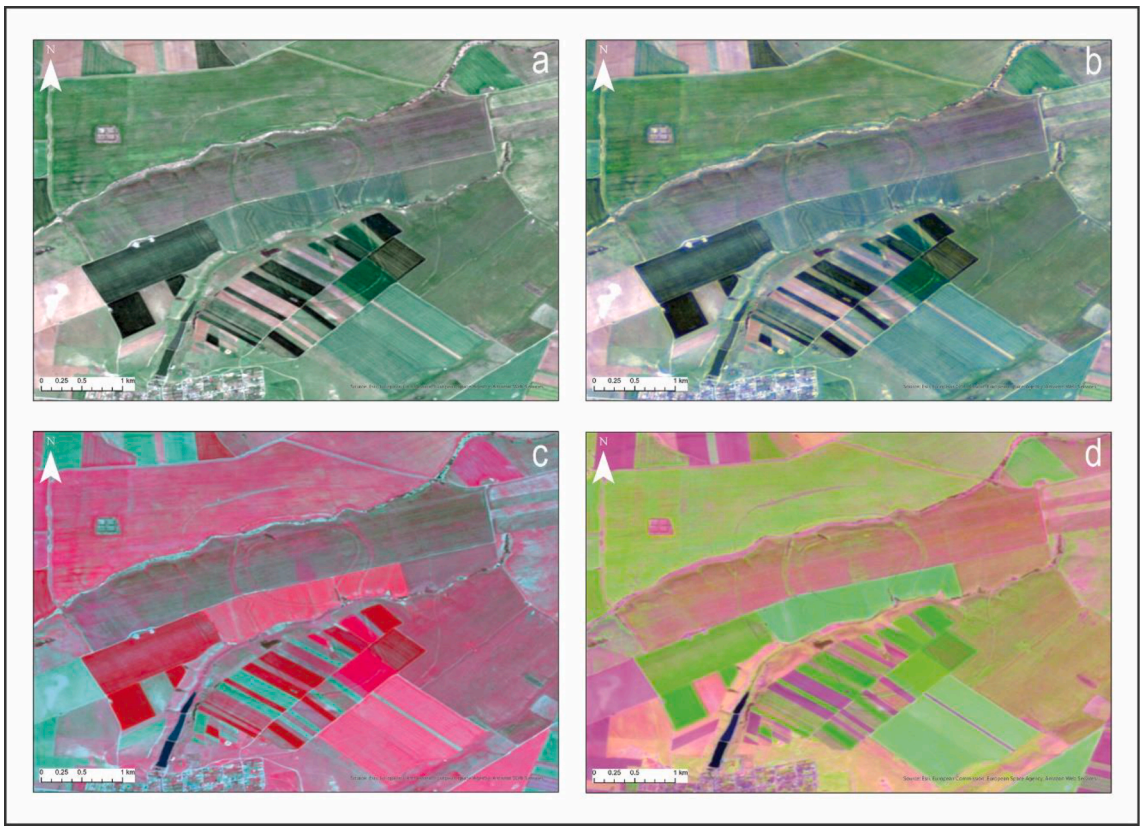

Fig. 6. Various pseudo colour composites of the Sentinel 2 image at the Corneşti-Iarcuri archaeological site. (a) Natural colour composite (red, green, blue, bands 4, 3, 2). (b) Pseudo colour composite (red, green, coastal/aerosol, bands 4, 3, 1). (c) Pseudo colour composite (NIR, R, G, bands 8, 4, 3). (d) Agricultural pseudo colour composite (shortwave IR-1, near-IR, blue, bands 11, 8, 2). (For interpretation of the references to colour in this figure legend, the reader is referred to the web version of this article.)

method uses the Esri algorithm, a weighted average, and an additional near-infrared band to create its pan-sharpened output bands. An adjustment value (ADJ) is calculated based on the weighted average to determine the output values. The weights for the multispectral bands are defined by the overlap of the multispectral bands' spectral sensitivity curves with the panchromatic band, providing relative weights. Therefore, a normalization procedure is needed. The multispectral band most overlaps the panchromatic band and is given the most weight. In contrast, a weight of zero is assigned to a multispectral band that does not overlap with the panchromatic band (ArcGIS Pro, 2022).

Pan-sharpened 15-m resolution pseudo colour composites were created for interpretation purposes. In addition, nine different vegetation indices, including those of the NDVI and the SR, were applied. Equations for the vegetation indices used in the study are shown in Table 2 (equations 2–10). Vegetation indices have also been applied to the Sentinel 2 images.

Furthermore, the so-called orthogonal equations were applied to the Landsat images, using the linear combinations proposed by Agapiou et al. (2013,2015) for the Landsat 5 sensor. Since the Landsat 5 sensor shares similar – nearly identical – spectral properties (spectral response filters and wavelength range) with those of Landsat 9, the same equations can be adopted for the latest sensor. The linear equations are shown in equation 11.

$$CC1 = -0.01^{*}\, p_{Blue} + 0.06^{*}\, p_{Green} - 0.01^{*}\, p_{Red} + 1.00^{*}\, p_{NIR}.$$

$$CC2 = -0.32^{*}\, p_{Blue} - 0.74^{*}\, p_{Green} + 0.58^{*}\, p_{Red} + 0.5^{*}\, p_{NIR}.$$

$$CC3 = -0.38^{*}\, p_{Blue} - 0.45^{*}\, p_{Green} - 0.80^{*}\, p_{Red} - 0.02^{*}\, p_{NIR} \quad [eq.\ 11].$$

CC1 refers to vegetation, CC2 to soil, and CC3 to crop marks, while p_{Blue}, p_{Green}, p_{Red}, and p_{NIR} refer to the visible and near-infrared spectral bands of the Landsat sensor (namely, the Bands 2–4 and Band 8) (Agapiou et al., 2015; Agapiou, 2017b).

The above products were then interpreted and cross-compared with existing archaeological data and reports from ground remote sensing investigation methods (geophysical campaigns).

4. Results

4.1. Pan-sharpened results

As mentioned earlier, four different pan-sharpened techniques were applied to downscale the Landsat 9 multispectral images up to 15-m resolution using the panchromatic band. Fig. 5 presents the results after applying the Gramm-Schmidt and the Brovey transformations. Despite the spectral distortion of the original multispectral image, the pan-sharpening techniques can enhance archaeological proxies and therefore support visual interpretation and other semi-automatic feature extraction techniques. Fig. 5-a shows the original Landsat 9 image at 30-m resolution over the archaeological site of Corneşti-Iarcuri, while Fig. 5-b and -c show the pan-sharpened Landsat 9 image using the Brovey and the Gramm-Schmidt techniques, respectively. As is evident, the curved features of the site become visible in the pan-sharpened algorithms, while the Gramm-Schmidt technique provides sharper results.

4.2. Pseudo colour composites

Pseudo colour composites using the different multispectral bands of the Landsat and Sentinel 2 sensors were then generated. RGB combinations can visualise three spectral bands at a time, assisting with the image interpretation and detection procedure of crop marks. Fig. 6 presents an example of this investigation applied to a Sentinel 2 image. Four different pseudo colour composites were generated using the

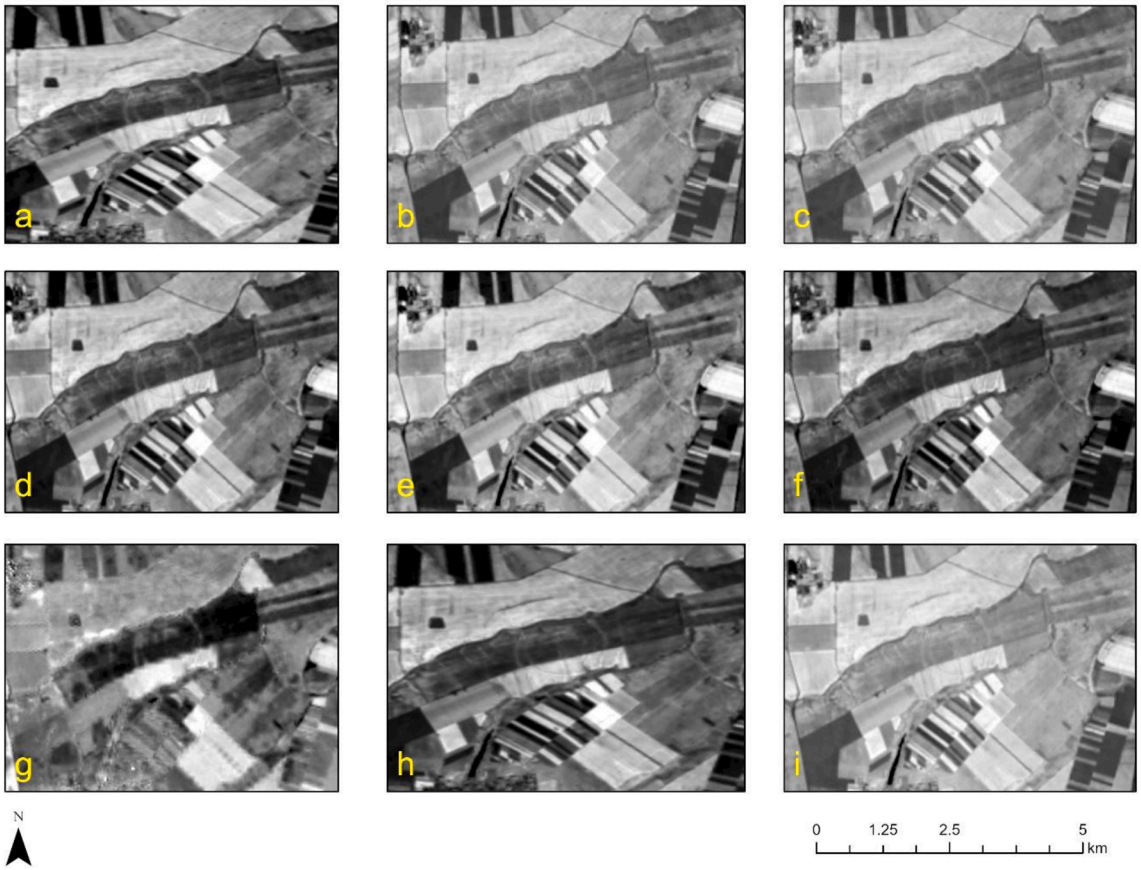

Fig. 7. Vegetation indices applied at the Corneşti-Iarcuri archaeological site using the pan-sharpened Landsat image. (a) NDVI; (b) Green NDVI; (c) SAVI; (d) TSAVI; (e) MSAVI; (f) PVI; (g) VARI; (h) MTVI2, and (i) SR. (For interpretation of the references to colour in this figure legend, the reader is referred to the web version of this article.)

spectral bands of Sentinel 2. Fig. 6-a indicates the so-called natural colour composite (red, green, blue, bands 4, 3, 2), while Fig. 6-b shows another pseudo colour composite based on the R, G, and coastal/aerosol spectral bands (4, 3, 1) of the sensor. Fig. 6-c indicates the NIR, R, G pseudo colour composite (namely, the spectral bands 8, 4, 3), and finally, Fig. 6-d shows the so-called agricultural pseudo colour composite based on the shortwave IR-1, NIR, and B bands (bands 11, 8, 2).

In all the pseudo colour composites of Fig. 6, the boundaries of the Corneşti-Iarcuri site are visible as they cross the different cultivated areas of the region. The ramparts can be easily spotted in the different spectral combinations. The contrast of these crop marks is quite strong and they can be differentiated from the cultivated background, thus allowing an almost complete understanding of the shape of the underground features. Similar findings were observed in other areas of interest, indicating the potential use of the medium resolution images through simple visual interpretations.

4.3. Vegetation indices results

As mentioned earlier, vegetation indices were implemented in both datasets. Fig. 7 presents the results for all indices applied at the Corneşti-Iarcuri archaeological site, while Fig. 8 shows similar findings over the Sântana area. While comparable results were obtained from all indices, it was evident that some of them could provide more detailed results of archaeological proxies than others. For instance, the Perpendicular Vegetation Index (PVI, Fig. 7-f) can enhance the crop mark features of the area better than the Visible Atmospherically Resistant Index (VARI, Fig. 7-g). Crop marks may discontinue from parcel to parcel due to different cultivation techniques, agricultural practices, soil properties, etc.

It should also be noted that in other areas, as in the cases of the Sântana and Corneşti-Iarcuri archaeological sites, findings might be different. Indeed, in Fig. 8, we can observe that the Visible Atmospherically Resistant Index (VARI, Fig. 8-g) and the Simple Ratio (Fig. 8-i) can distinguish crop marks better than all the other vegetation indices applied to the Landsat image.

This observation regarding the applicability of the vegetation indices and their performance in various archaeological sites has already been reported in the literature for other case studies. As also shown here, aligned with the literature review, the NDVI index can sometimes be problematic (see Fig. 8-a) in distinguishing crop marks compared to other known vegetation indices Vegetation indices were also applied to the 10-m resolution Sentinel 2 images. An example of applying the Simple Ratio (SR) vegetation index to an image of the archaeological site of Sântana is depicted in Fig. 9. Fig. 9-a shows the NIR, R, G pseudo colour composite, while Fig. 9-b presents the results after implementing the SR index. Despite the improved spatial resolution of the Sentinel-2 image, the interpretation of crop marks in the SR image remains difficult.

4.4. Orthogonal equations results

The so-called orthogonal equations were used to improve the overall findings and further enhance any crop marks. This was also done to investigate whether these equations could be adopted in areas outside the Eastern Mediterranean region, where they were initially developed. Orthogonal equations are designed to enhance the spectral distance between three distinct spectral groups: healthy vegetation, soil, and crop marks. Orthogonal equations are a result of a 3-D rotation of the PCA eigenvectors of the spectral space of the image.

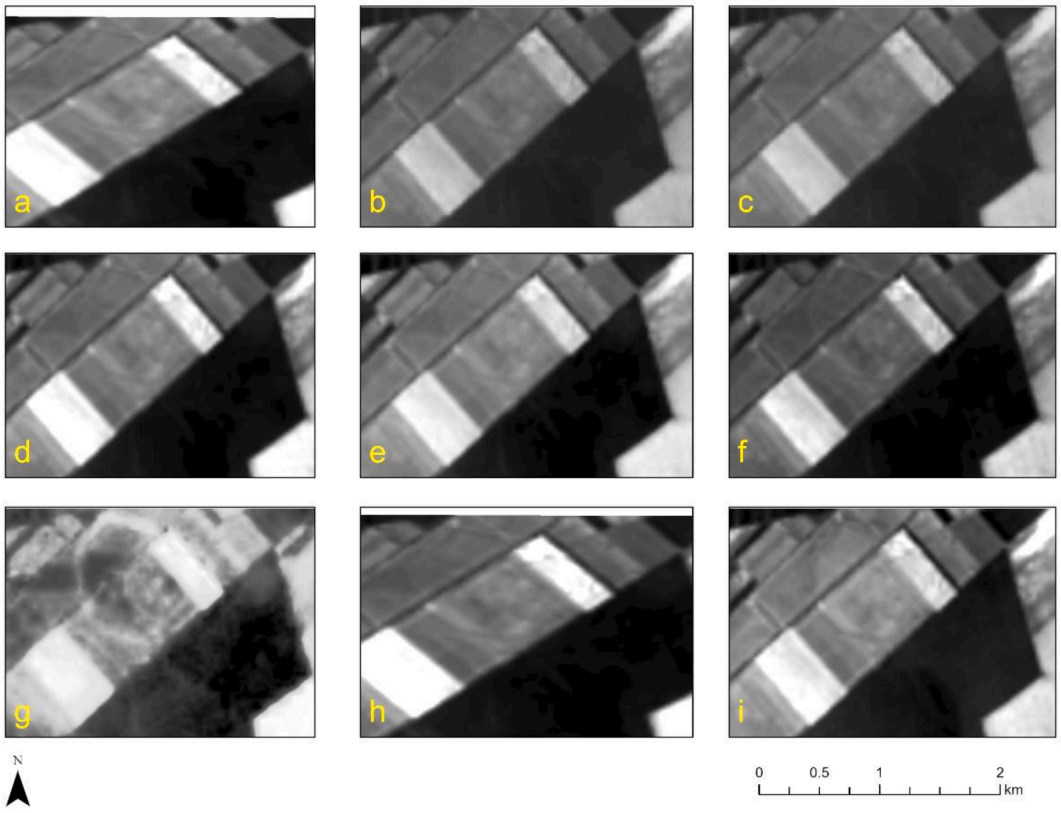

Fig. 8. Vegetation indices applied at the Sântana archaeological site using the pan-sharpened Landsat image. (a) NDVI; (b) Green NDVI; (c) SAVI; (d) TSAVI; (e) MSAVI; (f) PVI; (g) VARI; (h) MTVI2, and (i) SR. (For interpretation of the references to colour in this figure legend, the reader is referred to the web version of this article.)

Examples from the areas of the Corneşti-Iarcuri and Sântana archaeological sites are depicted in Figs. 10 and 11, respectively. Fig. 10-a shows the Landsat image over the Corneşti-Iarcuri site, while Fig. 10-b, -c, and -d show the three components of the orthogonal equations after implementing them, namely, the vegetation, soil, and crop mark components, respectively. Fig. 10-e shows the RGB composite of the three previously mentioned components, while Fig. 10-f shows the panchromatic band of the Landsat image. Fig. 11 demonstrates in a similar order the results over the Sântana area.

It was found that the application of the orthogonal equations, especially the "crop mark", can enhance the overall signal of the image and, therefore, support image interpretation. At the Sântana archaeological site, the crop mark component (Fig. 11-d) can reveal other crop marks in the southern part of the site that were not detectable in the original pan-sharpened Landsat image (Fig. 11-a) or the panchromatic band of the same sensor (Fig. 11-f). Fig. 12 indicates the crop mark component of both sites (i.e., Corneşti-Iarcuri and Sântana) on a larger scale. The defensive system is visible in both images.

5. Discussion

5.1. Evaluation of the results

Several broadband vegetation indices were applied to Sentinel 2 and Landsat 9 images. As demonstrated above, vegetation indices were not always successful in enhancing crop marks for the Corneşti-Iarcuri and Sântana sites. For instance, in Sântana (Fig. 8), while most of the indices tended to fail – including NDVI and Green NDVI – the VARI index was able to discriminate linear and curved features. This observation contrasts with the findings of the Corneşti-Iarcuri area (Fig. 7). In this study, the VARI index tended to oversaturate the spectral signal, while the former two indices (NDVI and Green NDVI) were able to enhance the crop marks.

The study's outcomes are aligned with existing knowledge from the literature. The findings highlight that some vegetation indices may be used successfully to detect crop marks formed by buried archaeological remains. However, at the same time, other vegetation indices may fail and provide blurry outcomes. Indeed, as stated already in other studies (Agapiou et al., 2012; Calleja et al., 2018), other, less known vegetation indices – such as, in our case study, the VARI index – can assist in the detection of crop marks. In addition to this, the PVI index (Figs. 7-f and 8-f) also demonstrated reliable performance in both areas. This comment is aligned with results from other applications for detecting crop marks (e.g., Pirowski et al., 2021).

The performance difference of the same vegetation indices in the two different case studies (Corneşti-Iarcuri and Sântana) can be explained by the different phenological cycles of the crops cultivated on top of the archaeological sites. Indeed, as both the Sentinel 2 and Landsat 9 images were not taken on the same date, the crop growth was not identical for both areas. Other parameters, like the different soil conditions and the micro-climate of the areas, should also be considered (Abate et al., 2019).

5.2. Fusion of data

It is therefore difficult to quantify the overall performance of the individual sensors (i.e., Sentinel 2 and Landsat 9) and directly compare the results generated from the different processing techniques. As the spatial scope of satellite-based investigation methods is extensive (with limited archaeological visibility), these studies are primarily designed to fuse different sources of information for a better understanding of particular landscapes. As the individual products from both the Sentinel and Landsat sensors were presented in the previous section, here we have attempted to combine the overall findings.

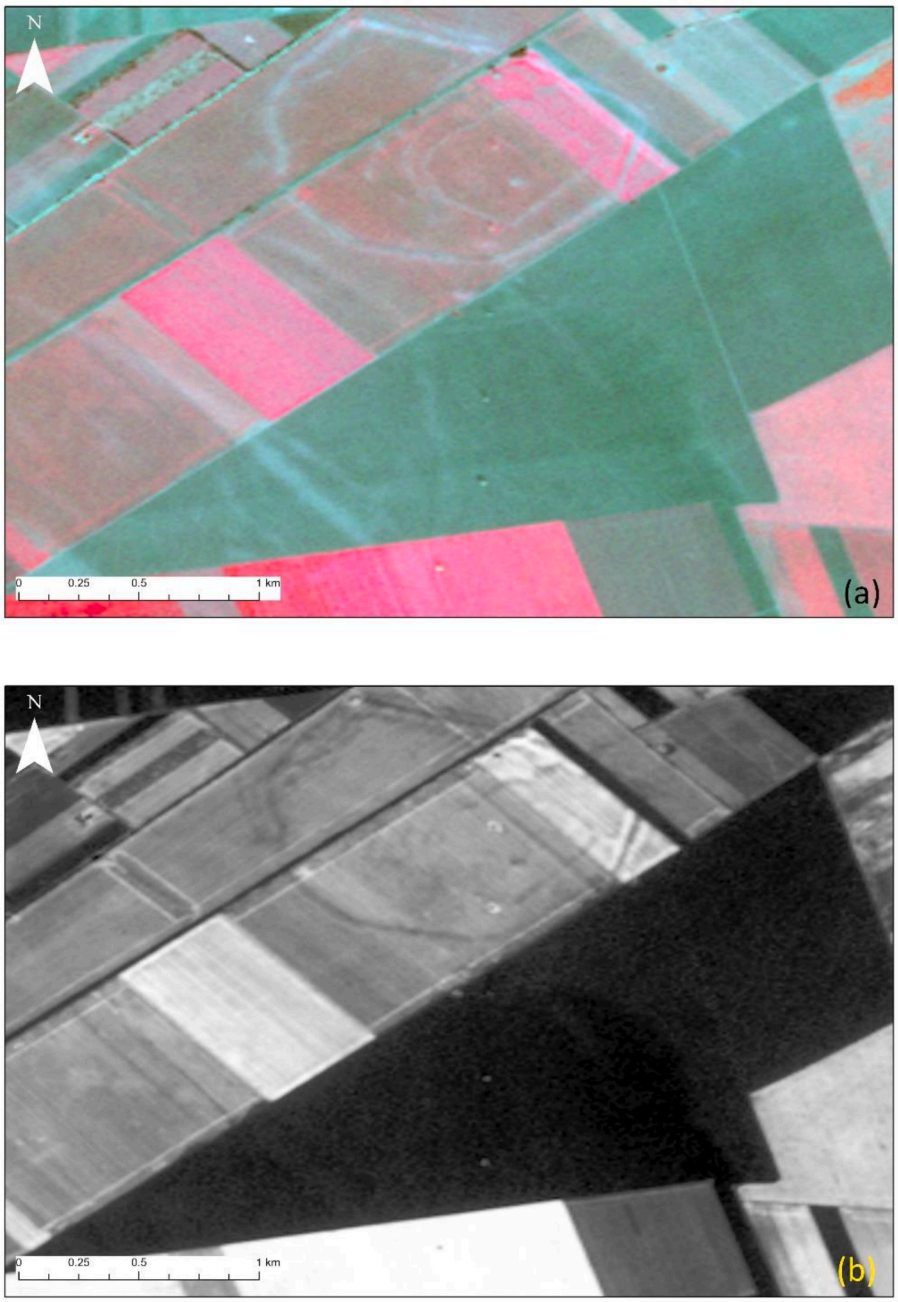

Fig. 9. Vegetation indices applied at the Sântana archaeological site using a Sentinel 2 image. NIR, R, G pseudo colour composite (a) and SR index (b).

For this reason, we have elaborated on some promising outcomes from Landsat 9 and Sentinel 2 images, and specifically the crop mark component of the pan-sharpened Landsat 9 image (see Fig. 12-b), the panchromatic band of Landsat 9 (Fig. 11-f), and the Simple Ratio (SR) index of the Sentinel 2 image over the Sântana area (Fig. 9-b). For further analysis, these results were rescaled with values between 0 and 1 (normalisation). A pseudo-colour composite of this combination is shown in Fig. 13. The black arrows in the figure indicate linear and curved features (known and unknown archaeological proxies – see next section). A step forward from this simple combination of the three different components (i.e., the crop mark of Landsat 9, the panchromatic band of Landsat 9, and the SR index of the Sentinel 2) is the calculation of the Principal Component Analysis (PCA) of this composite. As the individual layers are normalised, the PCA can provide a new 3-D layer of information with uncorrelated components. Indeed, as shown in Fig. 14, the second principal component (PC2) from the PCA analysis of the three components can further enhance the outlines of the Sântana site, based on the cumulative information of all components (crop mark, panchromatic, and SR).

5.3. Confirmation of archaeological evidence and new anomalies

Even if using vegetation indices algorithms are not always satisfying, specific information can be drawn when combined with archaeological results. We successfully used archaeology as a proxy and linked most of the anomalies to specific archaeological structures at both sites (Cornești-Iarcuri and Sântana – Cetatea Veche). The fortification system of the discussed sites is clearly visible on both Sentinel and Landsat images, owing to the impressive sizes of these sites. As a result, extensive geophysical results (magnetic surveys) and large archaeological excavations at both sites confirm the fortification lines. Even the ramparts and ditches that are highly levelled, such as the fourth fortification line

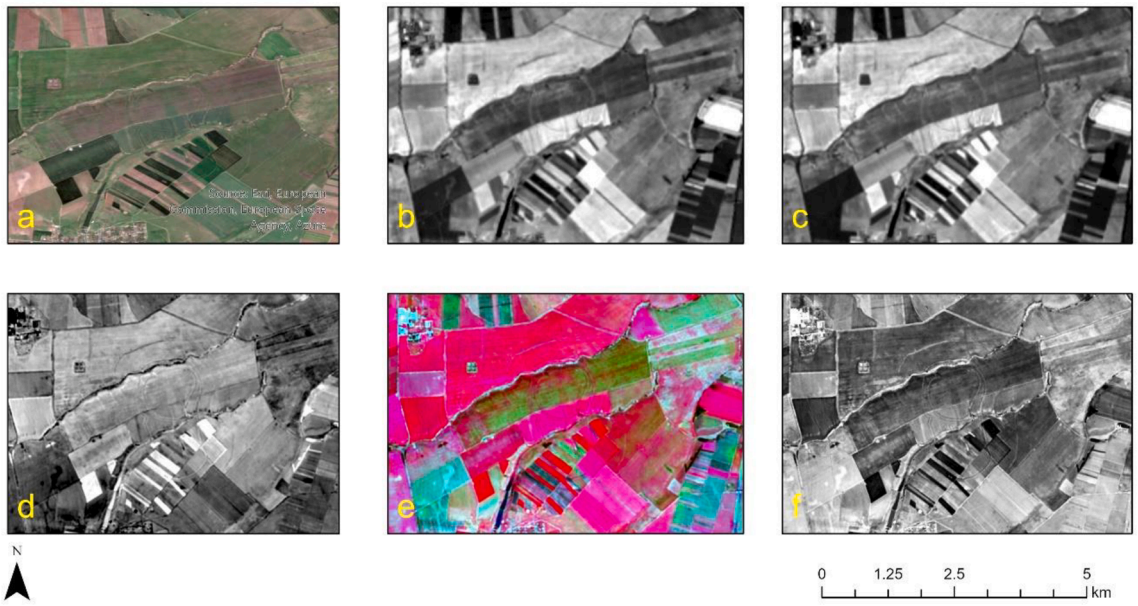

Fig. 10. (a) Landsat 9 image over the Corneşti-Iarcuri area; (b) Vegetation component; (c) Soil component; (d) Crop mark component; (e) RGB composite of vegetation, soil, and crop mark components; and (f) panchromatic band.

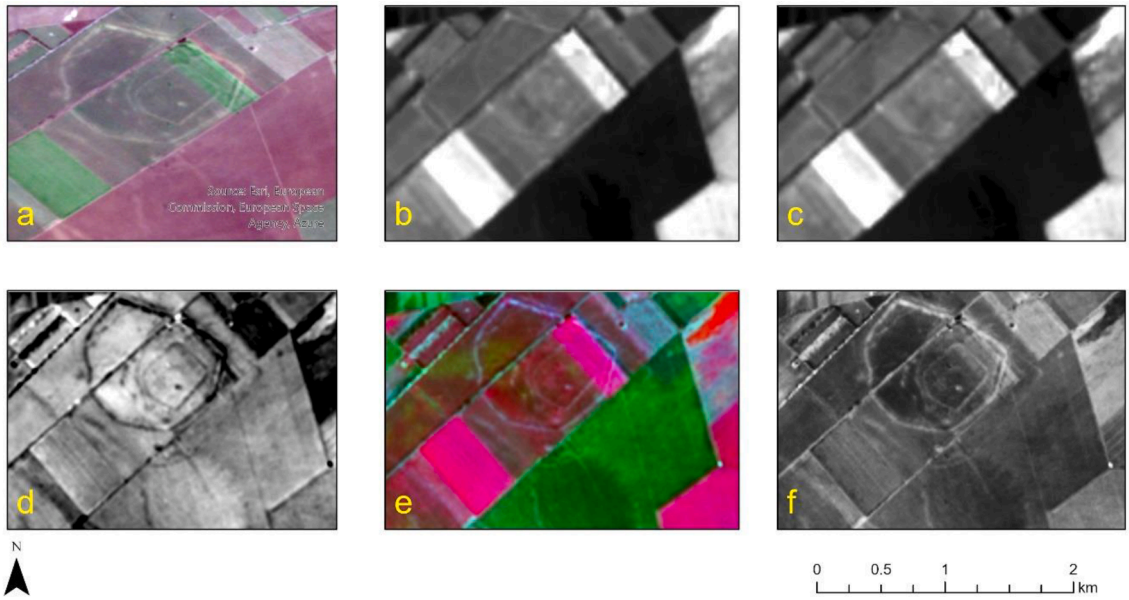

Fig. 11. (a) Landsat 9 image over the Sântana area; (b) Vegetation component; (c) Soil component; (d) Crop mark component; (e) Pseudo colour RGB composite of the vegetation, soil, and crop mark components; and (f) Panchromatic band.

at Cornești-Iarcuri or the outer southern fortification line in Sântana – Cetatea Veche, are well individualized. The existence of the fortification lines is not novel information as they had already been archaeologically documented through remote sensing (Micle et al., 2006; Micle et al., 2009) and excavations (Gogâltan and Sava, 2010; Szentmiklosi et al., 2011, 2016).

However, a closer look at the Cornești crop mark map indicates an anomaly in front of the main gate on the second line of fortifications, which could be another defence element to strengthen that fortification's entrance point (Fig. 15, green circle). Other geophysical discovered structures can also be spotted in the investigated satellite images. At Sântana – Cetatea Veche, for example, the location of the so-called megaron-type edifice and other dwellings can be clearly identified (Fig. 16). Outside the main wall, several other rectangular structures can be seen. These are most likely other houses that were later reinforced with an additional fortification line which is visible as a distinctive linear crop mark (Fig. 14).

The most astounding outcomes of our investigation can be found in Cornești-Iarcuri (Fig. 15). Fortunately, the site benefited from an intensive magnetic survey, which generated amazing results, which were published previously (Szentmiklosi et al., 2011). Some of the features are visible on satellite images as well. However, due to the site's scale, it was hard to forecast where the magnetic survey should be disseminated to identify its most significant features. One of these regions is located on two agricultural lots west of the main gate on the second fortification line. A series of rectangular anomalies (Fig. 15, red arrows), some of which are quite large, can be seen here. These structures are located between the third and fourth ramparts. Because of their

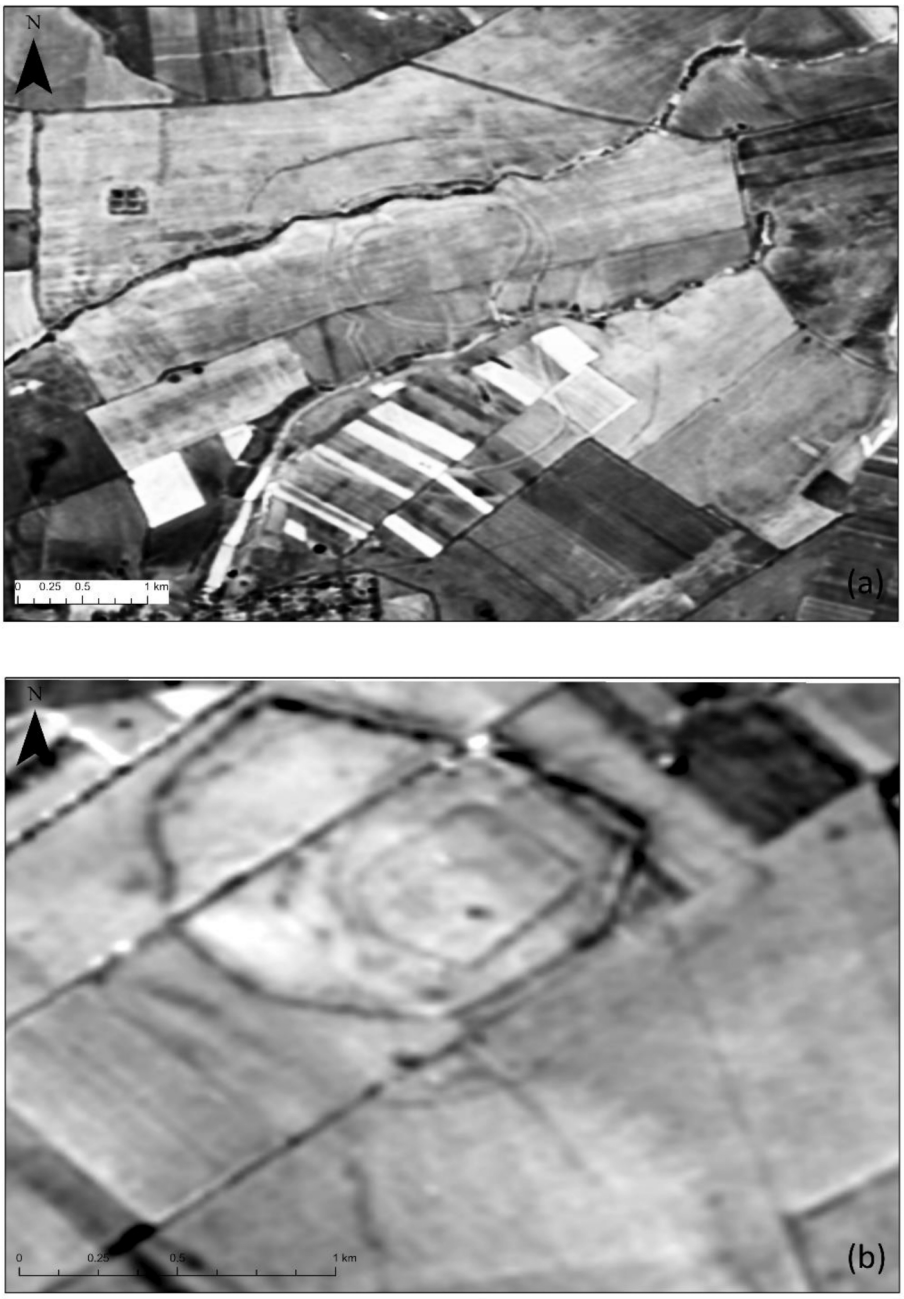

Fig. 12. (a) Crop mark component over the Cornești-Iarcuri area and (b) the crop mark component at the Sântana area.

shape, we can assume that these anomalies are large dwellings or important structures related to the fortification. In addition, next to the fourth fortification line, another series of anomalies stand out in this area (Fig. 15, blue circle). Closer inspection reveals a large rectangular structure, most likely ditches, enclosing a series of minor anomalies that could also be dwellings. The location of these anomalies suggests a pattern of distribution. One of the archaeological excavations conducted over the fourth fortification line in that area can also be seen. At the moment, it is unclear whether this is related to the main Bronze Age fortification, and only future archaeological surveys will be able to establish the chronological and spatial relationships. However, the findings of our investigation within this region of the site may prompt archaeologists to take a closer look at these structures, confirming or denying their existence in the field. Given that this is still a large area, we believe that conducting a systematic magnetic survey within the boundaries of the site could yield significant archaeological results. Aside from the anomalies observed here, other regions with crop mark anomalies could be noticed on the fortification's eastern side (Fig. 15, yellow circles).

The use of medium-resolution multispectral images in conjunction with a combined and comparative remote-sensing approach to study archaeological landscapes within and beyond the bronze age mega fortifications could reveal important archaeological findings that would otherwise be missed even by extensive field surveys. Based on the findings of this work and another recent remote-sensing paper about the megafort of Csanádpalota-Juhász T. tanya in Hungary (Agapiou et al. 2023), landscape archaeologists may apply similar approaches on a larger scale. Other sites in southwestern Romania were explored (with extremely good archaeological results) using satellite remote sensing approaches (Dorogostaisky and Hegyi, 2017; Hegyi et al., 2020; Stavilă et al., 2020; Agapiou et al., 2023).

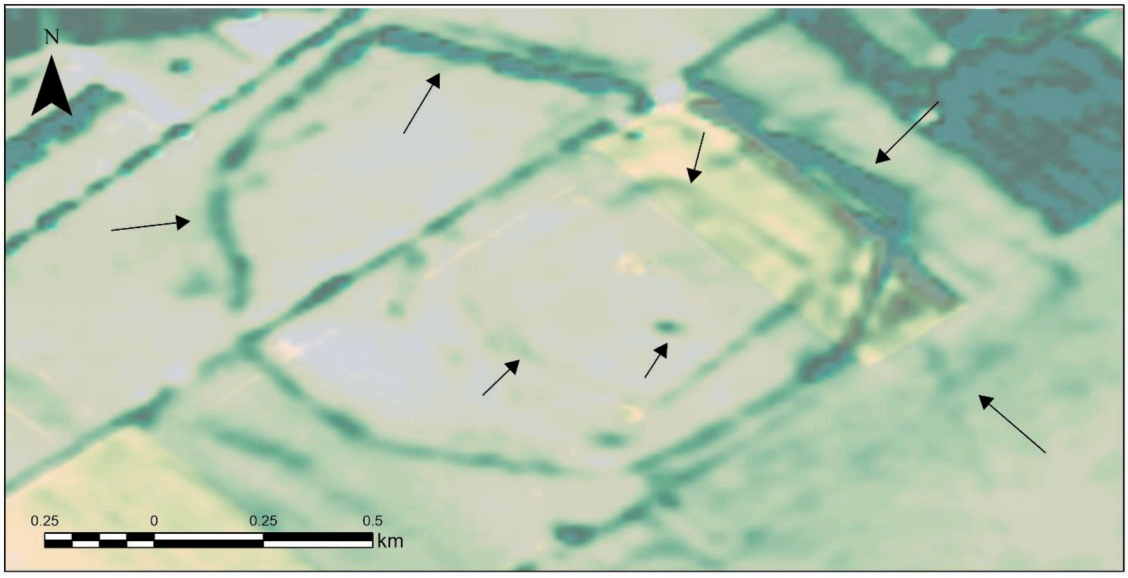

Fig. 13. RGB composite over the Sântana area, using the crop component of Landsat 9, the panchromatic band of Landsat 9, and the Simple Ratio (SR) index from the Sentinel 2 image. Black arrows indicate archaeological proxies.

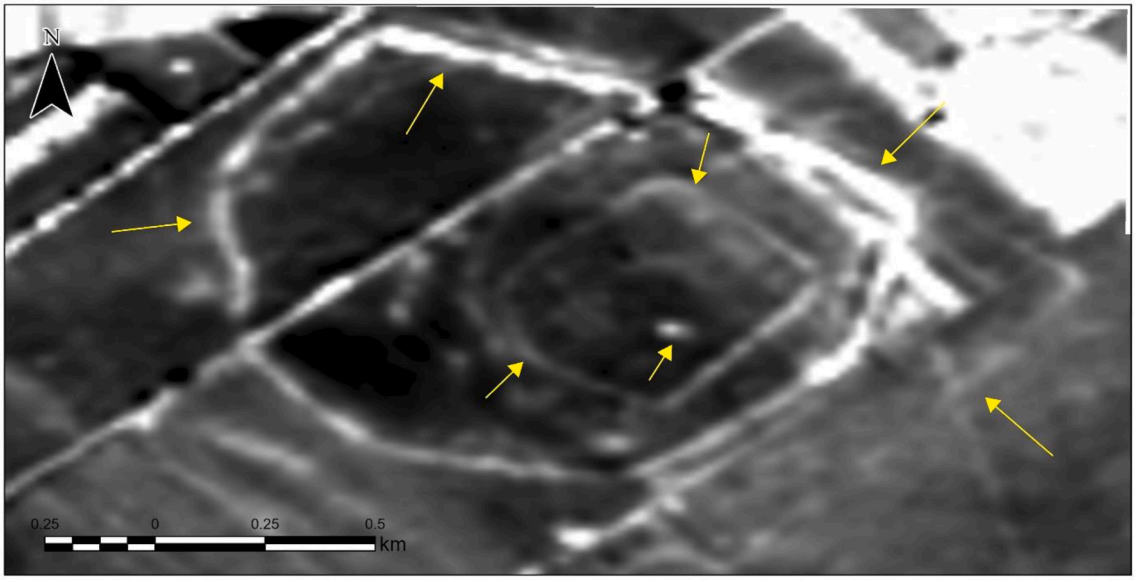

Fig. 14. The second principal component (PC2) over the Sântana area, after the PCA analysis of the crop component of Landsat 9, the panchromatic band of Landsat 9, and the Simple Ratio (SR) index from the Sentinel 2 image. Yellow arrows indicate archaeological proxies. (For interpretation of the references to colour in this figure legend, the reader is referred to the web version of this article.)

6. Conclusion

In this study, open-access and freely distributed medium resolution satellite images, namely the Sentinel 2 and the newly launched Landsat 9 optical sensors were used to investigate potential archaeological proxies. For this purpose Europe's most extensive fortifications (Corneşti-Iarcuri and Sântana – Cetatea Veche sites) were used as case studies. Different image techniques were applied such as vegetation indices, orthogonal transformations, and pan-sharpening techniques.

The findings of this study indicate that medium-resolution satellite images may be used for large archaeological sites to determine the area's broader context. Multispectral medium-resolution satellite images can also assess potential locations for future non-invasive shallow-ground geophysics research. While the resolution of these images is not always desirable, proper analysis can reveal structures that are not visible through traditional visual inspections. The study indicated that even if specific algorithms fail to uncover archaeological proxies, others will. Of course the spatial resolution of the sensors always remain a critical parameter that needs to be taken into consideration.

In the case of Cornești-Iarcuri, our analyses identified a series of possible overlooked archaeological features during the site's non-invasive research. These findings may encourage archaeologists to pursue additional work in the indicated regions. In Sântana – Cetatea Veche, we correlated multispectral data anomalies with specific archaeological structures identified during the geophysical survey. The megaron-type structure which is currently being excavated was visible on the Landsat and Sentinel data, as were other impressive structures within the fortification.

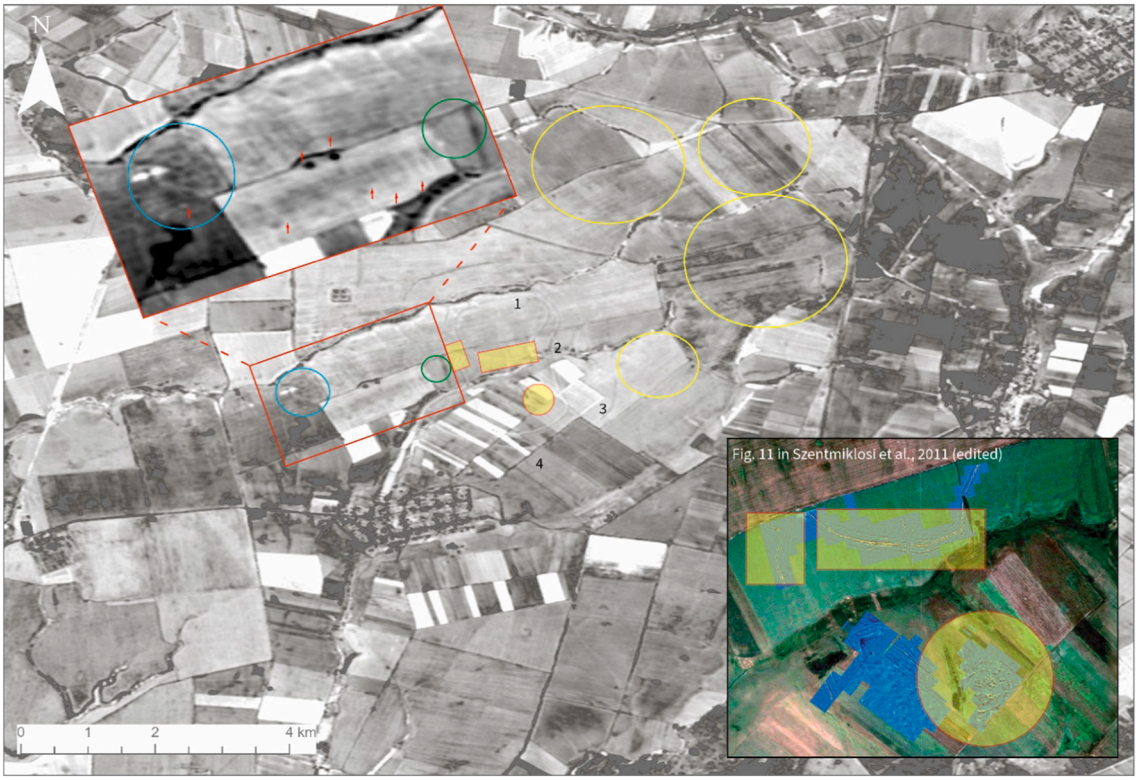

Fig. 15. Crop marks at Cornești-Iarcuri: Red-outlined polygons with yellow fill: archaeological features identified by geophysical surveys (bottom right of the figure: an edited screenshot of Fig. 11 from Szentmiklosi et al., 2011, highlighting the fortification system and other structures); Red arrows (zoom in: area west of the main gate on the second fortification line) indicate possible archaeological features such as large buildings/dwellings; Blue circle: a large structure (possibly ditches) enclosing a series of topographically organized features neighbouring the fourth line of fortification); Green circle: a structure on the third rampart, directly in front of the main gate, on the second line of fortification – possibly an additional fortification element; Other regions with potential archaeological features such as dwellings/houses or households are indicated by yellow circles/ellipses. (For interpretation of the references to colour in this figure legend, the reader is referred to the web version of this article.)

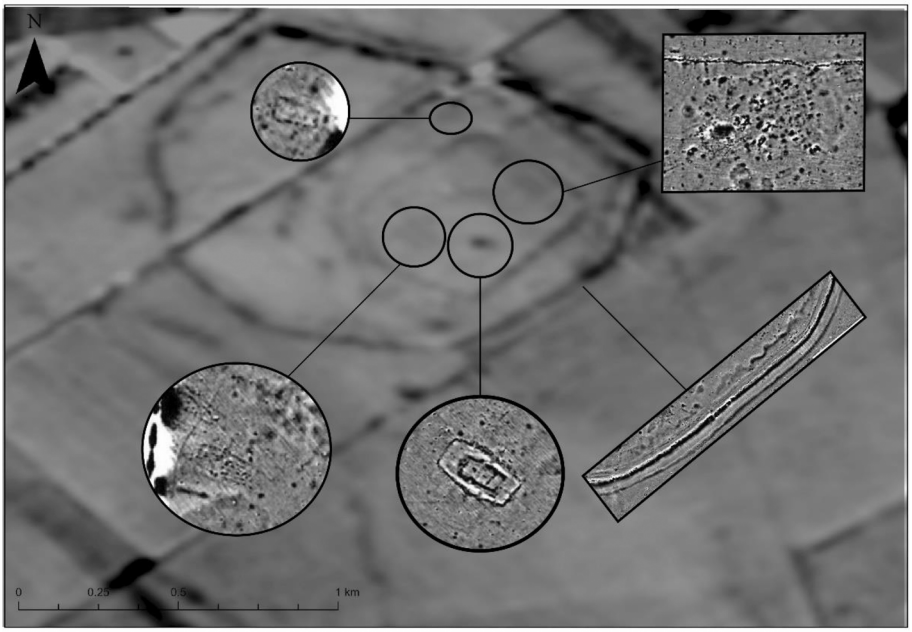

Fig. 16. Crop marks at Sântana – Cetatea Veche: The magnetic survey results were used to cross-reference several visible anomalies. When compared to other fainter anomalies indicating other dwellings, the megaron-type house (located in the first enclosure) produced a strong anomaly. Magnetic positive anomalies of low intensity characterize the faint crop marks (magnetic map (edited) after Gogâltan et al., 2019, Fig. 5).

Additionally, the study demonstrates how specific algorithms for processing multispectral data can provide numerous benefits for archaeological interpretation. For instance, pan-sharpening aids in increasing the contrast between various archaeological features (ramparts, ditches, etc). Pan sharpening techniques are considered as a necessary step for medium resolution image processing in archaeological research, as with this approach the spatial resolution of the images can be improved. It is also worth noting that using orthogonal equations to define crop marks is beneficial for studying archaeological sites via satellite remote sensing. Indeed, several crop marks were able to be determined using this transformation.

The study documents the inability of vegetation algorithms to provide important archaeological information for large-scale sites that encompass numerous agricultural plots with diverse plant cultures. Finally, our study can facilitate archaeologists studying these sites by providing future research directions.

CRediT authorship contribution statement

Athos Agapiou: Conceptualization, Methodology, Software, Writing – original draft, Writing – review & editing. **Alexandru Hegyi:** Conceptualization, Methodology, Software, Writing – original draft, Writing – review & editing. **Florin Gogâltan:** Writing – original draft, Writing – review & editing. **Andrei Stavilă:** Writing – original draft, Writing – review & editing. **Victor Sava:** Writing – original draft, Writing – review & editing. **Apostolos Sarris:** Writing – review & editing. **Cristian Floca:** Writing – review & editing. **Leonard Dorogostaisky:** Writing – review & editing.

Declaration of Competing Interest

The authors declare that they have no known competing financial interests or personal relationships that could have appeared to influence the work reported in this paper.

Data availability

Data will be made available on request.

Acknowledgements

A.H. would like to acknowledge PN-III-P1-1.1-PD-2019-0939, founded by UEFISCDI. A.A. would like to acknowledge the ENSURE project (Innovative survey techniques for detection of surface and sub-surface archaeological remains, CUT internal funding). Acknowledgements also are given for the use of open-access, freely distributed satellite datasets from Copernicus Open Access Hub (Sentinel 2 images) and EarthExplorer, available from the United States Geological Survey (Landsat 9 images).

References

Abate, N., Elfadaly, A., Masini, N., Lasaponara, R., 2020. Multitemporal 2016–2018 Sentinel-2 data enhancement for landscape archaeology: the case study of the Foggia Province, Southern Italy. Remote Sens. 12, 1309. https://doi.org/10.3390/rs12081309.

Abate, N., Aromando, A., Lasaponara, R. 2019. Old Methods and New Technologies: A Multidisciplinary Approach to Archaeological Research in Sant'Arsenio (Salerno, Italy). Lecture Notes in Computer Science (Including Subseries Lecture Notes in Artificial Intelligence and Lecture Notes in Bioinformatics), 11622 LNCS. https://doi.org/10.1007/978-3-030-24305-0_24.

Abate, N., Lasaponara, R., 2019. Preventive archaeology based on open remote sensing data and tools: the cases of Sant'Arsenio SA and Foggia FG, Italy. Sust. Switzerland 11 (15). https://doi.org/10.3390/su11154145.

Agapiou, A., 2017a. Remote sensing heritage in a petabyte-scale: satellite data and heritage Earth Engine© applications. Int. J. Digital Earth 10 (1), 85–102. https://doi.org/10.1080/17538947.2016.1250829.

Agapiou, A., 2017b. Orthogonal equations for the detection of archaeological traces demystified. JAS Rep. 14, 792–799. https://doi.org/10.1016/j.jasrep.2016.07.004.

Agapiou, A., Hegyi, A., Stavilă, A., 2023. Observations of archaeological proxies through phenological analysis over the Megafort of Csanádpalota-Juhász T. tanya in Hungary Using Sentinel-2 Images. Remote Sens. 15 (2), 464.

Agapiou, A., Hadjimitsis, D.G., Alexakis, D.D., 2012. Evaluation of broadband and narrowband vegetation indices for the identification of archaeological crop marks. Remote Sens. 4 (12), 3892–3919. https://doi.org/10.3390/rs4123892.

Agapiou, A., Alexakis, D.D., Sarris, A., Hadjimitsis, D.G., 2013. Orthogonal re-projection of spectral bands using medium and high resolution satellite images for the detection of archaeological crop marks. Remote Sens. 5 (12), 6560–6586. https://doi.org/10.3390/rs5126560.

Agapiou, A., Alexakis, D.D., Sarris, A., Hadjimitsis, D.G., 2014. Evaluating the potentials of Sentinel-2 for archaeological perspective. Remote Sens. 6, 2176–2194. https://doi.org/10.3390/rs6032176.

Agapiou, A., Alexakis, D.D., Sarris, A., Hadjimitsis, D.G., 2015. Linear 3-D transformations of Landsat 5 TM satellite images for the enhancement of archaeological signatures during the phenological of crops. Int. J. Rem. Sens. 361, 20–35. https://doi.org/10.1080/01431161.2014.990646.

Agapiou, A., Lysandrou, V., 2015. Remote sensing archaeology: tracking and mapping evolution in scientific literature from 1999–2015. J. Archaeol. Sci. Rep. 4, 192–200.

ArcGIS Pro. Fundamentals of pan sharpening. <https://pro.arcgis.com/en/pro-app/2.6/help/data/imagery/fundamentals-of-pan-sharpening-pro.htm> (Accessed on 15 April 2022).

Argyrou, A., Agapiou, A., 2022. A review of artificial intelligence and remote sensing for archaeological research. Remote Sens. 14 (23), 6000. https://doi.org/10.3390/rs14236000.

Baret, F., Guyot, G., 1991. Potentials and limits of vegetation indices for LAI and APAR assessment. Remote Sens. Environ. 35, 161–173.

Calleja, J.F., Requejo Pagés, O., Díaz-Álvarez, N., Peón, J., Gutiérrez, N., Martín-Hernández, E., Cebada Relea, A., Rubio Melendi, D., Fernández Álvarez, P., 2018. Detection of buried archaeological remains with the combined use of satellite multispectral data and UAV data. Int. J. Appl. Earth Obs. Geoinf. 73 https://doi.org/10.1016/j.jag.2018.07.023.

Chen, F., Lasaponara, R., Masini, N., 2015. An overview of satellite synthetic aperture radar remote sensing in archaeology: from site detection to monitoring, J. Cult. Herit., ISSN 1296-2074. <https://doi.org/https://doi.org/10.1016/j.culher.2015.05.003>.

Dorogostaisky, L., Hegyi, A., 2017. Noi ipoteze de lucru pentru cercetarea epocii bronzului în Banat (II). Un posibil complex de fortificații și așezări în arealul localităților Variaș-Satchinez (jud. Timiș). ArheoVest. Honorem Doina Benea 5, 747–770.

Ehlers, M., Klonus, S., Åstrand, J.P., Rosso, P., 2010. Multi-sensor image fusion for pansharpening in remote sensing. Int. J. Image Data Fusion 1, 25–45. https://doi.org/10.1080/19479830903561985.

Fanti, R., Gigli, G., Tapete, D., Mugnai, F., Casagli, N., 2013. Monitoring and modelling slope instability in cultural heritage sites. Landslide Sci. Pract.: Risk Assess. Manage. Mitig. 6 https://doi.org/10.1007/978-3-642-31319-6_62.

Gitelson, A.A., Kaufman, Y.J., Merzlyak, M.N., 1996. Use of a green channel in remote sensing of global vegetation from EOS-MODIS. Remote Sens. Environ. 58, 289–298.

Gitelson, A.A., Stark, R., Grits, U., Rundquist, D., Kaufman, Y., Derry, D., 2002. Vegetation and soil lines in visible spectral space: a concept and technique for remote estimation of vegetation fraction. Int. J. Remote Sens. 23, 2537–2562.

Gogâltan, F., Sava, V., 2010. Sântana Cetatea Veche – a Bronze Age Earthwork on the Lower Mureș. Complex. Muzeal Arad, Israel 2010, 99.

Gogâltan, F., Sava, V., Krause, R., 2019. Sântana-Cetatea Veche. A Late Bronze Age mega-fort in the Lower Mureș Basin in Southwestern Romania. In: Hansen, S., Krause, R. (Eds.), Materialisation of Conflicts. Proceedings of the Third International LOEWE Conference, 24th–27th September 2018 in Fulda Hesse, Germany. Universitätsforsch. Prähist. Arch. 346. Habelt-Verlag, Bonn, pp. 191–221.

Haboudane, D., Miller, J.R., Pattey, E., Zarco-Tejada, P.J., Strachan, I., 2004. Hyperspectral vegetation indices and novel algorithms for predicting green LAI of crop canopies: Modeling and validation in the context of precision agriculture. Remote Sens. Environ. 90, 337–352.

Harding, A., 2017. Cornești-Iarcuri and the rise of mega-forts in Bronze Age Europe. In: Heeb, B., Szentmiklosi, A., Krause, R., Wemhoff, M. (Eds.), Fortifications: The Rise and Fall of Defended Sites in Late Bronze and Early Iron Age of South-East Europe. Staatliche Museen zu Berlin, Berlin, 11–13 November 2015, pp. 9–14.

Hegyi, A., Sarris, A., Curta, F., Floca, C., Forțiu, S., Urdea, P., Stavilă, A., 2020. Deserted medieval village reconstruction using applied geosciences. Remote Sens. 12 (12), 1975.

Holliday, V.T., Gartner, W.G., 2007. Methods of soil P analysis in archaeology. Journal of Archaeological Science 34 (2). https://doi.org/10.1016/j.jas.2006.05.004.

Hritz, C., 2014. Contributions of GIS and satellite-based remote sensing to landscape archaeology in the Middle East. J. Archaeol. Res. 22, 229–276. https://doi.org/10.1007/s10814-013-9072-2.

Huete, A.R., 1988. A soil-adjusted vegetation index (SAVI). Remote Sens. Environ. 25 (3), 295–309. https://doi.org/10.1016/0034-4257(88)90106-X.

Johnson, A.B., Scheyvens, H., Shivakoti, R.B., 2014. An ensemble pansharpening approach for finer-scale mapping of sugarcane with Landsat 8 imagery. Int. J. Appl. Earth Obs. Geoinf. 33, 218–225.

Jordan, C.F., 1969. Derivation of leaf area index from quality of light on the forest floor. Ecology 50, 663–666.

Kirk, S.D., Thompson, A.E., Lippitt, C.D., 2016. Predictive modeling for site detection using remotely sensed phenological data. Adv. Archaeol. Pract. 41 (1), 87–101. https://doi.org/10.7183/2326-3768.4.1.87.

Laben, C.A., Brower, B.V., 2000. Process for Enhancing the Spatial Resolution of Multispectral Imagery Using Pan-Sharpening. U.S. Patent 6,011,875, 4 January 2000.

Lipo, C.P., Hunt, T.L., 2005. Mapping prehistoric statue roads on Easter Island. Antiquity 79 (303), 158–168. https://doi.org/10.1017/S0003598X00113778.

Luo, L., Wang, X., Guo, H., Lasaponara, R., Zong, X., Masini, N., Wang, G., Shi, P., Khatteli, H., Chen, F., et al., 2019. Airborne and spaceborne remote sensing for archaeological and cultural heritage applications: a review of the century (1907–2017). Remote Sens. Environ. 232, 111280.

Luo, L., Wang, X., Guo, H., 2022. Remote sensing archaeology: the next century. Innovation (Camb) 10;3(6), 100335. https://doi.org/10.1016/j.xinn.2022.100335.

Luo, L., Wang, X., Guo, H., Jia, X., Fan, A., 2023. Earth observation in archaeology: a brief review. Int. J. Appl. Earth Obs. Geoinf. 116, 103169.

Malhotra, H., Vandana, S., S., Pandey, R.,, 2018. Phosphorus nutrition: Plant growth in response to deficiency and excess. In: Fujita, M., Hasanuzzaman, M., Hawrylak-Nowak, B., Nahar, K., Oku, H. (Eds.), Plant Nutrients and Abiotic Stress Tolerance. Springer, Singapore, pp. 171–190. https://doi.org/10.1007/978-981-10-9044-8_7.

Masini, N., Lasaponara, R., 2020. Satellite and close range analysis for the surveillance and knowledge improvement of the Nasca geoglyphs. Remote Sens. Environ. 236 https://doi.org/10.1016/j.rse.2019.111447.

Micle, D., Măruia, L., Dorogostaisky, L., 2006. The earth works from Cornești - "Iarcuri" Orțișoara Village, Timiș County in the light of recent field research. An. Banat. SN 2006, XIV, 283–306.

Micle, D., Török-Oance, M., Măruia, L., 2009. The morpho-topographic and cartographic analysis using GIS and Remote Sensing techniques of the archaeological site Cornesti "Iarcuri", Timis County, Romania. In: Lasaponara, R., Masini, N. (Eds.), Advances on Remote Sensing for Archaeology and Cultural Heritage Management, Proceedings of the 1st International EARSeL Workshop CNR, Rome, Italy, 30 September–4 October 2008, pp. 387–393.

Molloy, B., Jovanović, D., Bruyère, C., Marić, M., Bulatović, J., Mertl, P., Horn, C., Milašinović, L., Mirković-Marić, N., 2020. A new Bronze Age mega-fort in Southeastern Europe: recent archaeological investigations at Gradište Iđoš and their regional significance. JFA 45 (4), 293–314. https://doi.org/10.1080/00934690.2020.1734899.

Nikolakopoulos, G.K., 2008. Comparison of nine fusion techniques for very high resolution data. Photogramm. Eng. Remote Sens. 74, 647–659.

Parcak, S.H., 2009. Satellite Remote Sensing for Archaeology. Routledge, London, 10.4324/9780203881460.

Opitz, R., Herrmann, J., 2018. Recent trends and long-standing problems in archaeological remote sensing. J. Comput. Appl. Archaeol. 1 (1), 19–41. https://doi.org/10.5334/jcaa.11.

Qi, J., Chehbouni, A., Huete, A.R., Kerr, Y.H., Sorooshian, S., 1994. A modified soil adjusted vegetation index. Remote Sens. Environ. 48, 119–126.

Richardson, A.J., Wiegand, C.L., 1977. Distinguishing vegetation from soil background information. Photogram. Eng. Remote Sens. 43 (12), 1541–1552.

Reid, S.H., 2016. Satellite Remote Sensing of Archaeological Vegetation Signatures in Coastal West Africa. African Archaeological Review 33 (2). https://doi.org/10.1007/s10437-016-9222-2.

Rouse, J.W., Haas, R.H., Schell, J.A., Deering, D.W., Harlan, J.C., 1974. Monitoring the vernal advancements and retrogradation (Greenwave effect) of nature vegetation. NASA/GSFC Type III Final Report. NASA/GSFC, Greenbelt, MD.

Sava, V., Gogâltan, F., 2017. The Bronze Age fortifications in Munar "Wolfsberg", Arad County. The 2014 and 2017 Archaeological Researches. AAR, 12, 75–100.

Sava, V., Gogâltan, F., 2022. Before the rise of the late bronze age mega forts. Ziridava. St. Archaeo. 36, 85–164.

Stavilă, A., Hegyi, A., & Craiovan, B. A., 2020, Non–invasive archaeological researches performed in the Middle Bronze Age settlement from Alioș–Valea Alioșu (Timiș County, Romania). Structures, chronology, and perspectives, Ziridava. St. Archaeo, pp. 169–188.

Szentmiklosi, A., Heeb, B.S., Heeb, J., Harding, A., Krause, R., Becker, H., 2011. Cornești-Iarcuri — a Bronze Age town in the Romanian Banat? Antiquity 85, 819–838. https://doi.org/10.1017/S0003598X00068332.

Szentmiklosi, A., Bălărie, A., Heeb, B., Urdea, P., 2016. Atestarea arheologică a celei de a patra linii de fortificații a cetății de epoca bronzului de la Cornești – Iarcuri jud. Timiș. MCA (Serie Nouă) 12, 105–114.

Szeverényi, V., Czukor, P., Priskin, A., Szalontai, C., 2017. Recent work on Late Bronze Age fortified settlements in southeast Hungary. In: Heeb, B., Szentmiklosi, A., Krause, R., Wemhoff, M. (Eds.), Fortifications: The Rise and Fall of Defended Sites in Late Bronze and Early Iron Age of South-East Europe. Staatliche Museen zu, Berlin, pp. 135–148.

Tapete, D., Cigna, F., 2018. Appraisal of opportunities and perspectives for the systematic condition assessment of heritage sites with Copernicus Sentinel-2 high-resolution multispectral imagery. Remote Sens. 10 (4) https://doi.org/10.3390/rs10040561.

Yang, S., Luo, L., Li, Q., Chen, Y., Wu, L., Wang, X., 2022. Auto-identification of linear archaeological traces of the Great Wall in northwest China using improved DeepLabv3+ from very high-resolution aerial imagery. Int. J. Appl. Earth Obs. Geoinf. 113, 102995 https://doi.org/10.1016/j.jag.2022.102995.

Zanni, S., de Rosa, A., 2019. Remote sensing analyses on sentinel-2 images: looking for Roman roads in Srem region Serbia. Geosci. Switzerland 91. https://doi.org/10.3390/geosciences9010025.

Zhang, Y., 2004. Understanding image fusion. Photogramm. Eng. Remote Sens. 70, 657–661.